ELSEVIER

PII: S0032-3861(98)00048-2

Polymer Vol. 39 No. 19, pp. 4579–4592, 1998

0032-3861/98/$19.00+0.00

Metastabilities of lamellar crystals of molecular complexes

L. Paternostre, P. Damman and M. Dosière*
Université de Mons-Hainaut, Laboratoire de Physicochimie des Polymères, Place du Parc, 20, B-7000 Mons, Belgium
(Received 2 October 1997; revised 21 November 1997; accepted 9 December 1997)

The molar stoichiometry and the crystal structure of four molecular complexes between poly(ethylene oxide) (PEO) and *p*-dichlorobenzene (PDCL), resorcinol (RES), hydroquinone (HYD) and *p*-nitrophenol (PNP) are compared. Even with a polymer weight fraction of 0.5, these molecular compounds form lamellar crystals when crystallized from the melt. The morphology of the lamellar crystals of these four PEO molecular complexes has been investigated in the early stages and after prolonged times of crystallization from the melt by time-resolved small-angle X-ray scattering coupled with wide-angle X-ray diffraction and differential scanning calorimetry. Non-integral-folded chain (NIFC) crystals are observed in the early stage of crystallization of PEO–RES and PEO–PNP molecular complexes from the melt. NIFC crystals of PEO–RES transform into integral-folded chain (IFC) and extended chain (EC) lamellar crystals with time. NIFC, 1-IFC and EC crystals can coexist in a sample of PEO–RES molecular complex. NIFC crystals of PEO–PNP do not transform into IFC or EC crystals even after long crystallization times or after heating until they melt. Stacks of IFC and EC crystals are present in the early stage of crystallization of PEO–HYD complexes at all the range of crystallization temperatures studied. The relative proportion of EC crystals of PEO–HYD increases with the crystallization temperature. PEO–PDCL forms only EC crystals at high crystallization temperatures ($T_c > 50$°C). The type and magnitude of the interactions between host and guest molecules account for the different lamellar morphologies of these four molecular complexes. PEO–RES forms banded and unbanded spherulites in the temperature range 20 to 55°C. Banded spherulites are metastable and transform into unbanded spherulites through a solid-phase transition.

(Keywords: supramolecular complexes; poly(ethylene oxide); lamellar crystals)

INTRODUCTION

It is well known that crystallizable synthetic polymers form lamellar crystals with folded chains[1]. The thickness of the lamellae is about 10 nm to a few tens of nm. It is often assumed that the majority of the crystallized macromolecules adopt an adjacent re-entry in lamellar crystals which indicates that the macromolecules deposit in quasi-independent layers during the crystallization. The crystal structure of poly(ethylene oxide) (PEO)[2,3] and the morphology of crystals of ethylene oxide (EO) oligomers have been extensively investigated[4–11]. PEO oligomers with weight-average molecular weights ranging between 2000 and 10 000 form lamellar crystals with either an integral number of folds ($n > 1$) or an extended chain (EC) conformation ($n = 0$)[4–11]. Raman longitudinal acoustic mode (LAM)[12,13], calorimetry[9–11] and SAXS[4–6] data indicate that the chain ends made up with OH groups are located at the surface of the lamellae and that the chain axes are perpendicular to these surfaces. A non-integral form of lamellar crystals of oligomers of PEO has been observed by LAM[13] and SAXS[14–17] studies. These non-integral-folded chain (NIFC) crystals are associated with the early stage of crystallization and transform with time into integral-folded chain (IFC) crystals. The transformation of the NIFC crystals into IFC crystals ($n = 0$ or 1) occurs either by a thickening or by a thinning process. Recently, Kim and Krimm[18] have shown by time-resolved LAM measurements that the chains are tilted with respect to the lamellar surfaces in NIFC crystals. On converting to extended ($n = 0$) or to one-fold ($n = 1$) chain crystals, the chains become perpendicular to the lamellar surface. These experimental results illustrate well the metastable morphology of polymeric crystals.

They are several reported cases where a solvent, on entering the crystal lattice of natural and synthetic polymers, becomes a component part of the polymer crystal structure[19]. In some cases, a molecular complex, i.e. a compound with a well-defined stoichiometry and possessing physical and chemical properties different from those of the two pure compounds, can be obtained.

PEO forms various crystalline molecular complexes with organic compounds such as urea[20–23], thiourea[22,23], *para*-dihalogenobenzenes[24–29], resorcinol (*meta*-dihydroxybenzene)[30–37], hydroquinone (*para*-dihydroxybenzene)[30,38,39], 2-methylresorcinol[36,37], 5-methylresorcinol[37,39] and *para*-nitrophenol[40–43].

The layered morphology of polymers crystals allows them to be host compounds in intercalates. If the distance between layers of folded chains can be slightly accommodated, small molecules with a given shape can intercalate between these layers. The shape of these empty parts is defined by the conformation of the macromolecular chains in the crystals. Assuming that the observed conformation

* To whom correspondence should be addressed

results only from intermolecular interactions, the following two cases are possible:

(1) The interaction between the host macromolecules and the guest molecules is not specific. The helical conformation of the polymer determines the size and the shape of the possible guest molecules. This is the case for all PEO–*para*-dihalogenobenzenes molecular complexes[24–29]. It is worth emphasizing that molecular complexes do not form between PEO and the other two isomers of dihalogenobenzenes, i.e. *ortho*- and *meta*-dihalogenobenzenes.
(2) Specific interactions, such as hydrogen bonds, occur between the oxygen ether of the PEO chains and the hydroxyl group of the benzenic molecule. In this category of compounds, PEO forms molecular complexes with resorcinol[30–37], hydroquinone[30,37–39], 2-methylresorcinol[36,37], 5-methylresorcinol[37,39] and *para*-nitrophenol[40–43].

This paper is devoted to the morphology of some typical molecular complexes such as PEO–*p*-dichlorobenzene (PEO–PDCL), PEO–resorcinol (PEO–RES), PEO–hydroquinone (PEO–HYD) and PEO–*p*-nitrophenol (PEO–PNP) where the specific interactions between host molecules and guest macromolecules are different in nature and magnitude. Some comments about the stoichiometry and the crystal structure of these four molecular complexes are necessary for the analysis of the morphological data, and will be therefore recalled briefly. The molecular complex PEO–RES will be used to illustrate how metastability can also occur at the level of the supralamellar structure, i.e. the coexistence in the same range of temperatures of two allotropic forms.

EXPERIMENTAL

The PEO molecular complexes were prepared by several successive meltings and recrystallizations of stoichiometric mixtures of the two components. PEO with a very high molecular weight (5×10^6) was obtained from Aldrich and was used to prepare stretched samples of PEO molecular complexes. An oligomer of ethylene oxide with an average molecular weight of 6000 (designated as PEO6K hereafter) was obtained from Hoechst and was used for the spherulitic crystallizations of PEO molecular complexes from the melt. Deuterated low-molecular-weight PEO ($< M_w > = 2000$) was purchased from MSD Isotopes (Montreal, Canada). Disubstituted benzenic molecules were purchased from Aldrich and were used as-received.

A Perkin Elmer differential scanning calorimeter (DSC4 model), operating under a nitrogen atmosphere and fitted with a TADS computing station and a low temperature cooling accessory, was used to record the melting curves. Benzoic acid and indium were used for calibration. Optical observations were made with a polarized optical microscope (Ortholux Leitz). The molecular complexes were crystallized in a Mettler FP82 hot stage monitored by an FP90 processor. Infrared spectra were recorded with a Brüker IFS 113V Fourier transform infrared spectrometer. Thirty-two coadded interferograms were scanned with a resolution of 2 cm^{-1}. Wide-angle (WAXD) and small-angle (SAXS) X-ray measurements were carried out with a Rigaku fine focus rotating anode generator delivering Cu Kα X-rays. A Kiessig camera with a pinhole collimation modified to record simultaneously the WAXD and the SAXS patterns was used. Time-resolved SAXS intensity measurements were carried out at the D24 X-ray beam line of the LURE-DCI synchrotron radiation facility (LURE, Centre Universitaire de Paris-Sud, Orsay, France).

RESULTS AND DISCUSSION

Phase diagram and stoichiometry of the molecular complexes

The phase diagram of PEO–*p*-dichlorobenzene (PEO6K–PDCL) displays a eutectic melting characterized by a weight fraction in *p*-dichlorobenzene of 0.045 and a melting temperature of 57.4 ± 0.5°C (*Figure 1*a)[44]. The melting temperature of the second eutectic is 50.3 ± 0.5°C, but its weight fraction cannot be determined with sufficient accuracy. The composition of the molecular compound (congruently melting compound) was determined by extrapolating the melting heats of the two eutectics to zero and leads to a weight fraction of 0.5 in *p*-dichlorobenzene. The melting temperature of the PEO–PDCL molecular complex is 83.5 ± 0.5°C. There are three molecules of *p*-dichlorobenzene for 10 E0 monomer units.

The phase diagram of the PEO–resorcinol (PEO6K–RES) complex also presents a bell-shaped domain but centred around a 2/1 molar stoichiometry (i.e. two EO monomer units for one resorcinol molecule) which separates two eutectic meltings (*Figure 1*b)[30–34]. The molar fraction of resorcinol and the melting temperature are, respectively, 0.10 and 43°C for the first eutectic and 0.49 and 86°C for the second eutectic. The melting temperature and the heat of fusion of the PEO–RES molecular complex are 93°C and 155 J g^{-1}, respectively.

The phase diagram of the PEO–*p*-nitrophenol (PEO–PNP) system is given in *Figure 1*c and is characteristic of a peritectic system[40] (incongruently melting complex) where the complex formed exhibits a transformation at a constant temperature, i.e. an incongruent melting (94.5 ± 0.5°C). Here, the stoichiometry of the molecular complex is derived from the intersection between the melting heat of the complex and the heat of the peritectic reaction against the weight ratio. The stoichiometry of the PEO–PNP molecular complex is found to be 0.68 (PNP weight ratio) which corresponds to a PNP molar ratio of 0.4, i.e. four *p*-nitrophenol molecules for six E0 monomer units.

The PEO–hydroquinone phase diagram has been established by several authors[30,37–39]. It has the characteristics of a eutectic–peritectic system showing the occurrence of a molecular complex. The PEO–hydroquinone phase diagram presents some similarities with the phase diagram of the PEO–PNP binary system. A direct observation of the phase diagram does not allow the determination of the stoichiometry of the molecular complex for such systems. The stoichiometry of the molecular complex previously proposed[30,37], corresponding to the weight fraction of the singular point (i.e. 42% w/w hydroquinone), is questionable. The phase diagram of the binary system PEO–hydroquinone obtained from our measurements[38,39] is given in *Figure 1*d. The use of the eutectic and peritectic heats of melting against the hydroquinone weight fraction gives a more precise value for the stoichiometry close to 0.53 for the PEO–HYD molecular complex, which corresponds to two EO monomers for one hydroquinone molecule. The melting temperature of the PEO6K–HYD molecular complex is 79°C.

The calorimetric data of these four molecular complexes are summarized in *Table 1*. The PEO molecular complexes

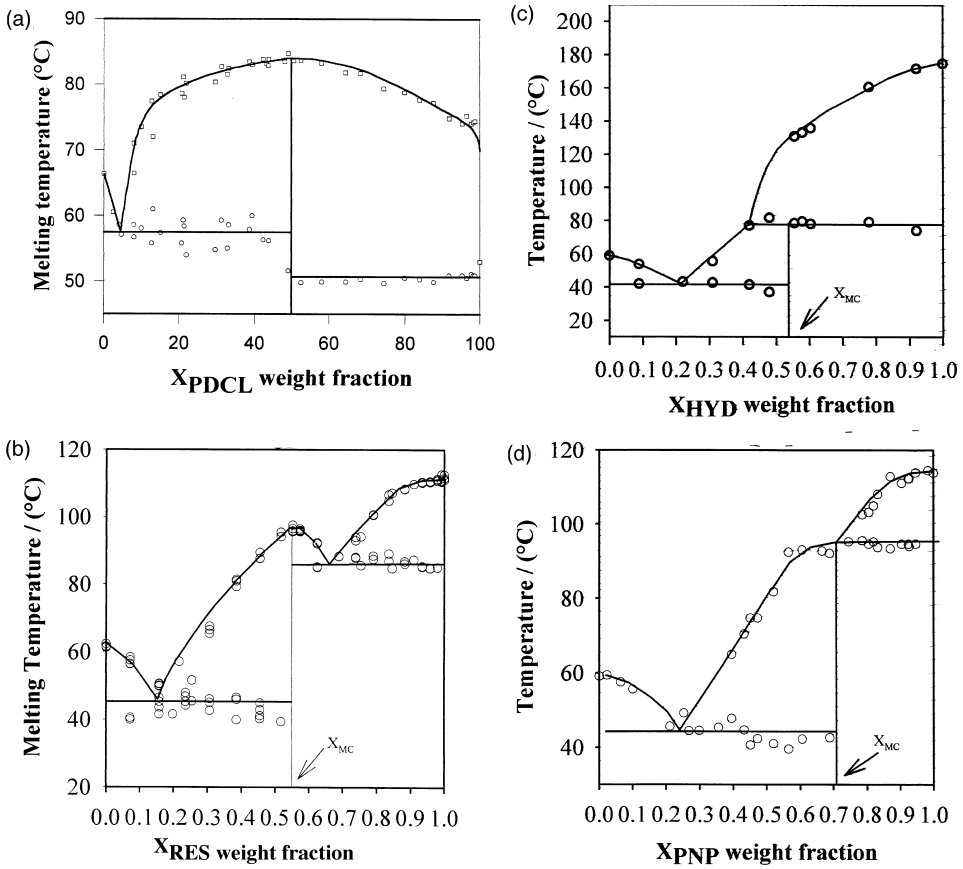

Figure 1 Phase diagram of molecular complexes between PEO6K and (a) *p*-dichlorobenzene, (b) resorcinol, (c) hydroquinone and (d) *p*-nitrophenol. *X* is the weight fraction of the benzenic compound. X_{MC} indicates the stoichiometry of the molecular complex

Table 1 Calorimetric data of poly(ethylene oxide) (PEO) and PEO molecular complexes

	PEO6K	PEO6K–PDCL	PEO6K–RES	PEO6K–HYD	PEO6K–PNP
T_{E1} (°C)	–	57.4	43	43	44
T_{E2} (°C)	–	50.3	86	79	95
X_{BZ}	–	0.5	0.53	0.53	0.68
Y	–	10/3	2/1	2/1	6/4
T_m (°C)	61.5	85	93–94	79	94.5
Type of melting	–	Congruent	Congruent	Incongruent	Incongruent

T_{E1} and T_{E2} are the melting temperatures of the eutectics. X_{BZ} is the weight stoichiometry of the molecular complex with respect to the disubstituted benzene molecule. *Y* is the ratio of the number of ethylene oxide units and disubstituted benzene molecules in the molecular complex. T_m is the melting temperature of the EC crystals of the PEO6K molecular complex

including the two isomers of dihydroxybenzenes have the same molar stoichiometry but quite different melting temperatures. As a rule, the melting temperature of these molecular complexes is about 20 to 30°C higher than the melting point of pure PEO6K oligomer.

Crystal structures of the molecular complexes

The preparation of macroscopic single crystals of PEO molecular complexes is not straightforward. The crystal structures of the molecular complexes (PEO–*p*-dichlorobenzene, PEO–RES (α-form), PEO–HYD and PEO–PNP) were determined from the analysis of two fibre patterns obtained from a stretched sample with the *c*-axis parallel to the fibre axis and from a large spherulite where one axis of the reciprocal unit cell (different from *c**) is along the radius of the spherulite. As large spherulites of PEO molecular complexes can be prepared, the WAXD pattern is recorded near the boundary of the spherulite. In this way, the spherulitic radii are nearly parallel in the region irradiated by the incident X-ray beam (the diameter of the X-ray incident beam was 0.3 mm).

The crystal structure of the PEO–PDCL molecular complex has been shown to be orthorhombic[28]. The unit cell contains 10 EO monomers and three *p*-dichlorobenzene molecules stacked along the *c*-crystallographic axis. The unit cell parameters are: $a = 1.648$ nm, $b = 0.951$ nm, *c* (chain axis) = 2.786 nm. The PEO chains adopt a 10/3 helical conformation which is very close to the 7/2 helical conformation of pure PEO. The molecular complex is made of alternating layers of PEO and *p*-$C_6H_4Cl_2$ (*Figure 2*a). Note that the arrangement of the guest *p*-dichlorobenzene molecules can be the same in successive layers or can alternate in two possible dispositions.

The stable form of the PEO–RES molecular complex is observed in stretched films and in unbanded spherulites. The stable form possesses an orthorhombic unit cell which

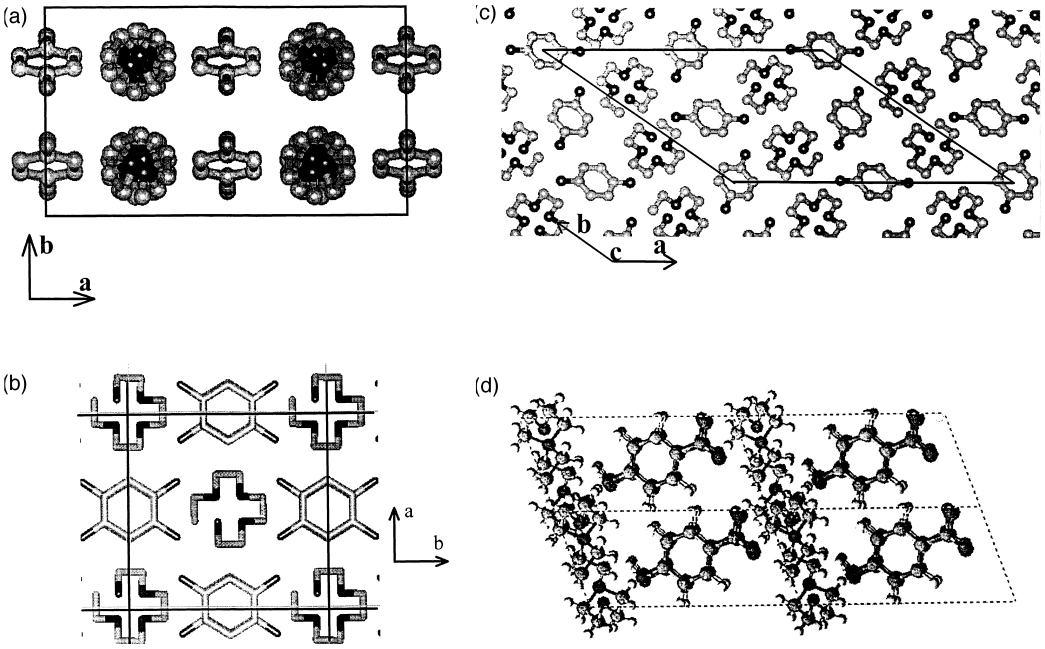

Figure 2 Projection of the unit cell of: (a) PEO–*p*-dichlorobenzene; (b); PEO–resorcinol; (c) PEO6K–hydroquinone; (d) PEO–*p*-nitrophenol

Table 2 Structural parameters of poly(ethylene oxide) (PEO) and PEO molecular complexes

	PEO	PEO–PDCL	PEO–RES	PEO–HYD	PEO–PNP
Reference	[1,2]	[24,28]	[34]	[39]	[40]
a (nm)	0.816	1.648	1.050	2.077	1.172
b (nm)	1.299	0.951	1.018	1.698	0.555
c (nm)	1.930	2.786	0.978	1.028	1.557
α (deg)	90.0	90.0	90.0	92.2	90.7
β (deg)	126.5	90.0	90.0	97.6	87.1
γ (deg)	90.0	90.0	90.0	34.72	104.0
Density (kg m^{-3})	1234	1341	1259	1290	1389
Crystalline system	Monoclinic	Orthorhombic	Orthorhombic	Triclinic	Triclinic
Spatial group	P_{21}/a–$C^5$2h	C_mC_{21}	P_{na21}	P_{-1}	P_{-1}
PEO conformation	7/2 helix	10/3 helix	4/1 helix	4/1 helix	$t_2gt_2gt_2g'$
Number of chains/unit cell	4	4	2	4	1
Stoichiometry (EO/BZ)	–	10/3	4/2	2/1	6/4
L_{ru} (nm)	1.930	2.786	0.978	1.028	1.557
M_{ru}	308.37	440.53	352.43	352.43	264.32

L_{ru} and M_{ru} are the length and the molecular weight of the repeat unit respectively

contains eight EO monomers and four resorcinol molecules (*Figure 2*b). The unit cell parameters are: $a = 1.050$ nm, $b = 1.050$ nm, c (chain axis) $= 0.976$ nm. The space group is P_{na21}. The PEO chains adopt a 4/1 helical conformation close to the 7/2 helix of pure PEO, but the periodicity along the chain axis is 0.976 nm and therefore the length of a PEO monomer unit is 0.244 nm in the molecular complex[34]. The determination of the structure of the metastable form found in banded spherulites is in progress.

The PEO–HYD molecular complex crystallizes in a triclinic unit cell[39]. The space group is P_{-1}. The unit cell parameters are: $a = 2.077$ nm, $b = 1.698$ nm, c (chain axis) $= 1.028$ nm, $\alpha = 92.2°$, $\beta = 97.6°$, $\gamma = 34.72°$. The experimental density of the molecular complex is 1.28 g cm^{-3}. As the molar stoichiometry of this complex is 2/1, the unit cell contains eight molecules of hydroquinone and 16 EO units. The PEO chains take on a 4/1 helical conformation. The crystal structure is shown in *Figure 2*c.

The crystal structure of the PEO–PNP molecular complex is triclinic with a P_{-1} space group[40]. The unit cell parameters are: $a = 1.172$ nm, $b = 0.555$ nm, c (chain axis) $= 1.557$ nm, $\alpha = 90.7°$, $\beta = 87.1°$, $\gamma = 104°$. The unit cell contains six EO monomers and four *p*-nitrophenol molecules stacked along the *c*-crystallographic axis. Here the PEO chains adopt a glide-type conformation ($t_2gt_2gt_2g'$) stabilized by hydrogen bonds which are established between the host and the guest molecules. This conformation differs completely from the 7/2 helix of pure PEO (*Figure 2*d).

Crystallographic data about these four PEO molecular complexes are summarized in *Table 2*. The PEO chains take on a helical conformation in three molecular complexes (PEO–PDCL, PEO–RES and PEO–HYD) very close to the 7/2 helix observed in pure PEO. Conversely, the

conformation of the PEO chain is quite different in the PEO–PNP molecular complex characterized by a triclinic unit cell and where the interactions between host and guest molecules are stronger than in the three other molecular complexes as will be explained further.

Morphology of lamellar crystals of some PEO molecular complexes crystallized from the melt

Time-resolved SAXS measurements have been performed to investigate the early stage of the crystallization of the four PEO–molecular complexes from the melt. Preliminary results obtained on PEO–RES and PEO–PNP molecular complexes have been recently published elsewhere[46]. Conventional SAXS, WAXD and DSC measurements were carried out on highly crystallized samples, i.e. samples having crystallized for more than 10 h at a given crystallization temperature. Results concerning these highly crystallized samples can be found elsewhere[43–45]. These two sets of experimental data will give information about possible metastable states occurring in the early stages of crystallization and in crystallized samples.

Time-resolved SAXS study of the crystallization of the PEO6K–PDCL molecular complex from the melt. Time-resolved SAXS measurements were carried out during the crystallization of the PEO6K–PDCL molecular complex from the melt at 45°C. The Lorentz corrected SAXS intensity curves obtained after various crystallization times are given in *Figure 3*a. Three maxima corresponding to long spacings equal to 42, 21 and 14 nm ($s = 0.0238$, 0.0476 and 0.0714 nm^{-1}, respectively) are already observed at the onset of crystallization (i.e. after 40 s). A fourth maximum appears after 80 s of the onset of crystallization. The four maxima correspond to the first four orders of a long spacing of 40.5 nm corresponding to the thickness of extended chains crystals of the PEO–PDCL molecular complex. As the intensity of the second order remains larger than the intensity of the first order in all SAXS intensity curves, the PEO–PDCL sample crystallized at 45°C consists of a mixture of extended chain (EC) and one-integral-folded chain (1-IFC) crystals even after a crystallization time of 700 s. This is further confirmed by the analysis of the corresponding correlation functions calculated from the SAXS intensity curves (*Figure 3*b). The analyses of the Lorentz corrected SAXS curves (*Figure 3*c) and of the correlation functions (*Figure 3*d) indicate that PEO–PDCL samples crystallized at 65°C contain only EC crystals.

Time-resolved SAXS study of the crystallization of the PEO–RES molecular complex from the melt. Time-resolved simultaneous WAXD and SAXS intensity curves were recorded at five crystallization temperatures (40, 50, 55, 65 and 70°C) after different times of crystallization. The ratio between the area of the crystalline peaks of the WAXD and the total area below the corrected WAXD intensity curve is proportional to the weight degree of crystallinity. These time-resolved WAXD intensity curves allow the determination of the evolution of the degree of crystallinity in the early stages of crystallization (*Figure 4*). The degree of crystallinity reaches its maximum value after 2 to 3 min, for crystallization temperatures of 50 and 65°C. The possible morphological modifications occurring after 3 min therefore involve solid-state transitions, such as thickening or thinning processes.

The Lorentz corrected SAXS intensity curves and the correlation functions corresponding to the crystallization of PEO6K–RES at 40°C are given in *Figure 5*a and *Figure 5*b, respectively. Only one scattering peak characterized by the

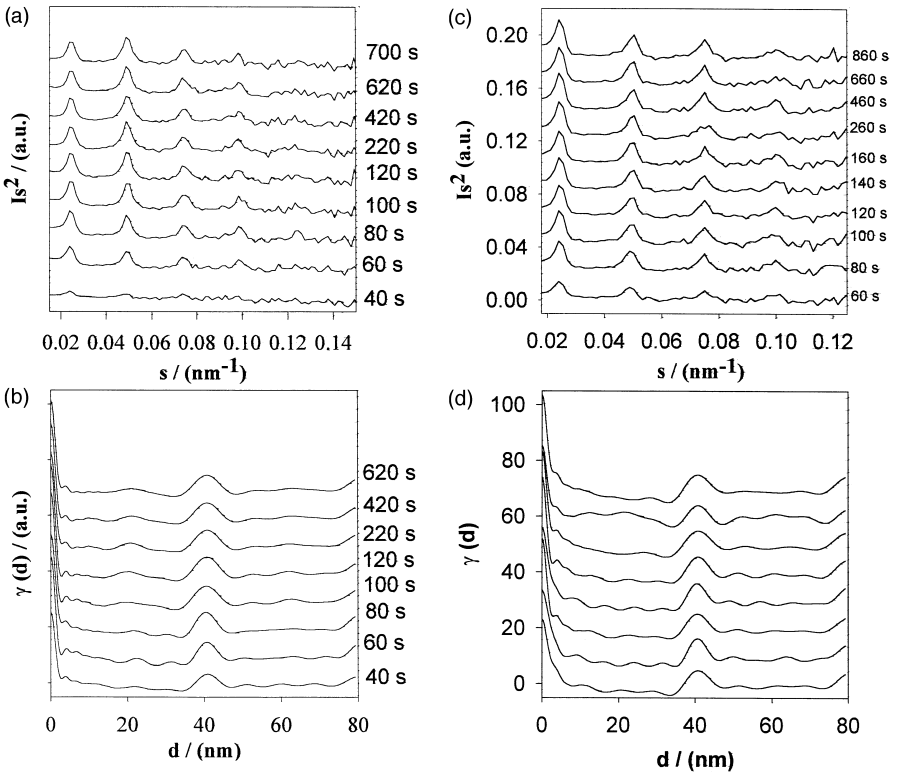

Figure 3 Crystallization of the PEO6K–*p*-dichlorobenzene molecular complex from the melt at (a) 45°C (c) 65°C: Lorentz corrected time-resolved SAXS intensity curves recorded at different times. The times are indicated on the right side of the figure (*s* is the value of the reciprocal vector). (b) and (d) are the corresponding correlation functions of SAXS curves given in (a) and (c) respectively

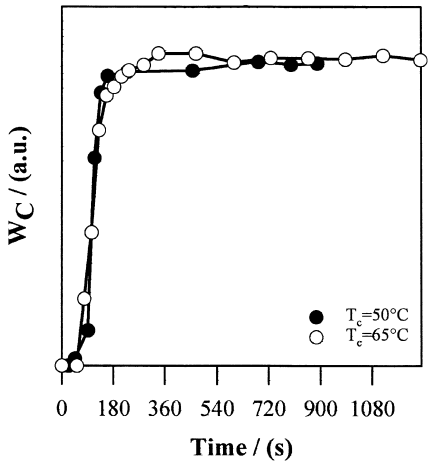

Figure 4 Degree of crystallinity of the PEO6K–RES molecular complex *versus* time during crystallization from the melt at 50 and 65°C

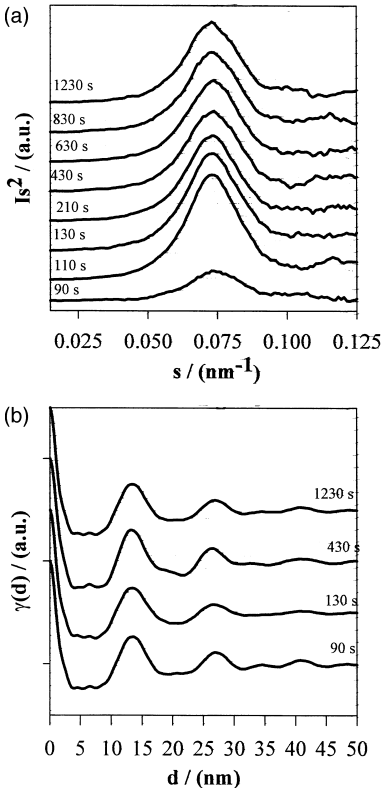

Figure 5 Crystallization of the PEO6K–RES molecular complex from the melt at 40°C: (a) Lorentz corrected time-resolved SAXS intensity curves recording at different times indicated on the left side of the figure; (b) correlation functions of some SAXS intensity curves given in (a)

same long spacing (13.7 nm) is observed in all SAXS curves. Since the thickness of EC crystals of PEO6K–RES is equal to 38.2 nm, this SAXS peak does not correspond to the thickness of 1-IFC or 2-IFC lamellar crystals, but instead to NIFC crystals. The growth of NIFC crystals from the melt is also supported by the very large width of the SAXS peak in the Lorentz corrected intensity curves.

The Lorentz corrected SAXS intensity curves and the correlation functions corresponding to the crystallization of PEO6K–RES at 65°C are given in *Figure 6*a and *Figure 6*b, respectively. Two maxima characterized by long spacings equal to 39.5 and 21 nm are observed in the scattering curve

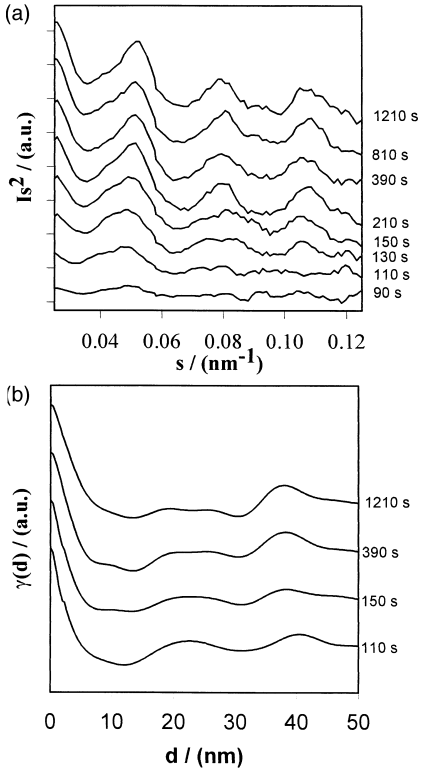

Figure 6 Crystallization of the PEO6K–resorcinol molecular complex from the melt at 65°C: (a) Lorentz corrected time-resolved SAXS intensity curves recording at different times indicated on the right side of the figure; (b) correlation functions of some SAXS intensity curves given in (a)

recorded after 90 s. The ratio of the area of the first and the second peak in the Lorentz corrected SAXS curve allows one to determine that the amount of folded chains crystals is larger than that of extended chain crystals. The presence of a shoulder on the left side of the second peak of the SAXS curves recorded after 110 to 390 s supports the occurrence of a relatively large distribution of thicknesses of the chain-folded crystals. After a crystallization time of 150 s, four peaks are observed in the Lorentz corrected SAXS curves. These four maxima correspond to the first four orders of the long spacing corresponding to the thickness of extended chain crystals (L = 39 nm). The PEO6K–RES molecular complex crystallizes in the early stage of crystallization from the melt as a mixture of NIFC, 1-IFC and EC lamellar crystals. The rate of transformation of NIFC crystals into IFC or EC increases with the crystallization temperature. This transformation, which occurs at temperatures well below the melting temperature of the molecular complex, corresponds to a solid-state transition.

Time-resolved SAXS study of the crystallization of the PEO–HYD molecular complex from the melt. The early stage of the crystallization of the PEO6K–HYD molecular complex was investigated at two crystallization temperatures: 40 and 60°C. The corrected SAXS curves and the corresponding correlation functions are given in *Figure 7*. PEO6K–HYD samples crystallized at low crystallization temperatures (40°C) contain a mixture of 1-IFC and 2-IFC crystals with thicknesses of 18.2 and 12.1 nm, respectively (*Figure 7*a and *Figure 7*b). EC crystals do not form at such low crystallization temperatures within the presently investigated crystallization times. At higher crystallization temperatures, e.g. 60°C, the growth of EC and 1-IFC crystals

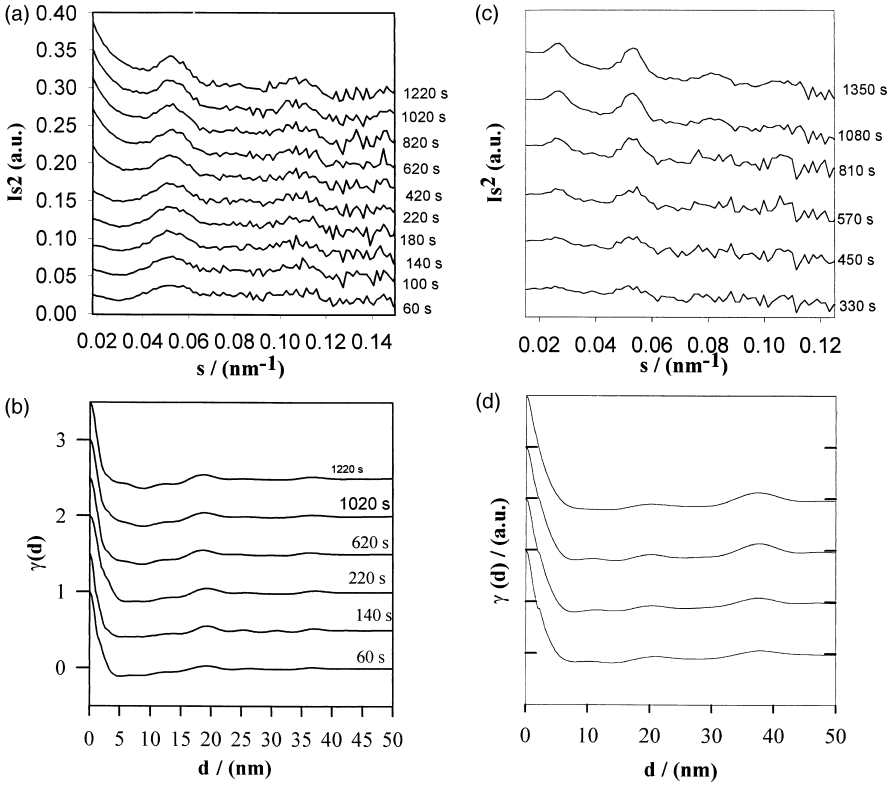

Figure 7 Crystallization of the PEO6K–hydroquinone molecular complex from the melt. Lorentz corrected time-resolved SAXS intensity curves recording at (a) 40°C and (c) 60°C and at different times indicated on the right side of the figure; (b) and (d) are correlation functions of some SAXS intensity curves given in (a) and (c) respectively

takes place concurrently in the early stage of crystallization (*Figure 7*c and *Figure 7*d). After a crystallization time of 1350 s, the relative amount of 1-IFC crystals is always larger than that of EC crystals.

Time-resolved SAXS study of the crystallization of the PEO–PNP molecular complex from the melt. Time-resolved simultaneous WAXD and SAXS intensity curves were recorded at four crystallization temperatures (50, 60, 65 and 70°C) at different crystallization times. The degree of crystallinity obtained from the WAXD intensity curve reaches its maximum value after a crystallization time of 180 s (*Figure 8*).

The Lorentz corrected SAXS intensity curves and the corresponding correlation functions are given in *Figure 9* and *Figure 10* for crystallization temperatures at 50 and 65°C, respectively. For both crystallization temperatures, the Lorentz corrected SAXS curves contain only one broad scattering peak which can be attributed unambiguously to the thickness of NIFC crystals.

The different morphological observations obtained from the analysis of time-resolved SAXS measurements are summarized in *Table 3*. IFC lamellar crystals are present in the early stage of crystallization of the PEO–PDCL molecular complex from the melt. The number of stacks of 1-IFC crystals is larger than that of EC crystals at low crystallization temperatures ($T_c \leq 45$°C). Above 45°C, EC lamellae crystallize immediately in the early stage of crystallization. The PEO6K–RES molecular complex crystallizes as NIF crystals in the early stage of crystallization. However, unlike the NIFC crystals observed in pure PEO oligomers, the NIFC crystals of PEO6K–RES are more stable and slowly transform into IFC or EC crystals. In fact, depending on the crystallization temperature and the

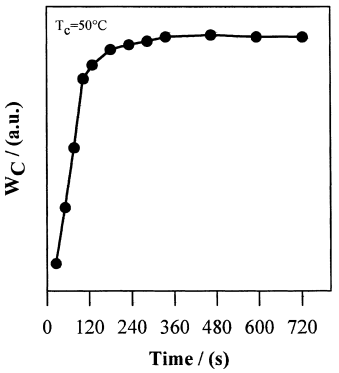

Figure 8 Degree of crystallinity of the PEO6K–*p*-nitrophenol molecular complex *versus* time during crystallization from the melt at 50°C

time, NIFC, IFC, EC lamellar crystals can be present in the same sample of the PEO–RES molecular complex. The PEO–HYD molecular complex crystallizes as 1-IFC and 2-IFC crystals between room temperature and 40°C. EC lamellar crystals of PEO–HYD grow from the melt at $T \geq 60$°C. The PEO–PNP molecular complex crystallizes from the melt as NIFC crystals which 'never' transform into IFC chains crystals even after very long crystallization times.

Morphology of the lamellar crystals of PEO molecular complexes obtained after prolonged crystallization times

PEO6K–PDCL molecular complex. Lorentz corrected SAXS intensity curves of PEO6K–*p*-$C_6H_4Cl_2$ crystallized at 30, 40, 50, 60 and 70°C for periods of time longer than 600 min exhibited six diffraction peaks (*Figure 11*a). The Bragg spacings are equal to 41, 20.5, 13.6, 10.25, 8.22 and

Table 3 Morphological data for lamellar crystals of PEO molecular complexes

Complex	ν_{OH} (cm^{-1})	Crystallization temperature T_c (°C)					
		25	40	50	60	65	70
PEO–PDCL	–		*x-IFC + EC*			*EC*	
		x-IFC = EC	*x*-IFC = EC	*x*-IFC ≪ E	EC	EC	EC
PEO–RES	3315		*NIFC*			*NIFC + xIFC + EC*	
		x-IFC < EC	*x*-IFC ≪ EC	*x*-IFC ≪ EC	*x*-IFC ⋘ EC	EC	EC
PEO–HYD	3365		*x*-IFC			*x*-IFC + EC	
		x-IFC = EC	*x*-IFC < EC	*x*-IFC < EC	*x*-IFC ≪ EC	*x*-IFC ≪ EC	*x*-IFC ≪ EC
PEO–PNP	3210				*NIFC*		
		NIFC	NIFC	NIFC	NIFC	NIFC	NIFC

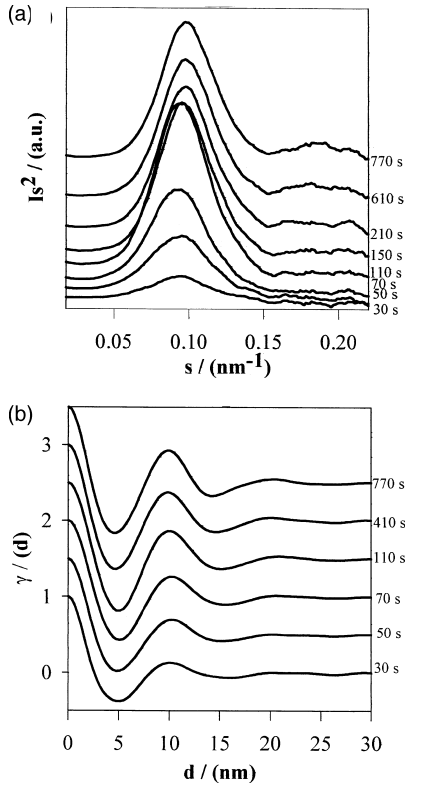

Figure 9 Crystallization of PEO6K–*p*-nitrophenol molecular complex from the melt at 50°C: (a) Lorentz corrected time-resolved SAXS intensity curves recording at different times indicated on the right side of the figure; (b) correlation functions of some SAXS intensity curves given in (a)

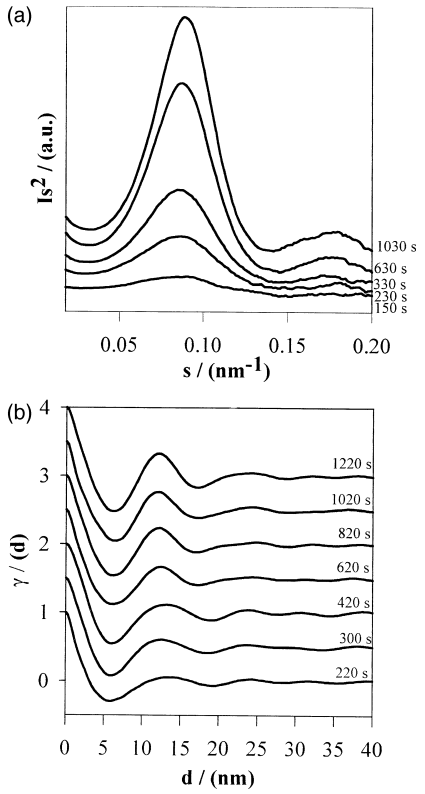

Figure 10 Crystallization of PEO6K–*p*-nitrophenol molecular complex from the melt at 70°C: (a) Lorentz corrected time-resolved SAXS intensity curves recording at different times indicated on the right side of the figure; (b) correlation functions of some SAXS intensity curves given in (a)

6.90 nm (*Figure 11*b). These peaks are the first six orders of a long spacing of 41 nm (calculated from the subsequent orders) corresponding to a full extended PEO6K chain having a 10/3 helical conformation of repeat period of 2.786 nm (*Table 2*). The correlation functions, calculated from the SAXS intensity curves, are given in *Figure 11*c and support this conclusion. A number-average molecular weight $< M_n^* >$ can be calculated from the long spacing according to the following relation: $<M_n^*> = (L/L_{ru}) \cdot M_{ru}$, where L, M_{ru} and L_{ru} are the lamellar thickness expressed in nm, the molecular weight of the repeat unit and its length, respectively[4–6]. From the values of M_{ru} and L_{ru} given in *Table 2*, the average molecular weight $< M_n^* >$ estimated from the long spacing $L = 41$ nm is equal to 6483, i.e. a slightly higher value than the value obtained by g.p.c. ($< M_n > = 5425$, $< M_w > = 5940$). The slight discrepancy between the values of the number-average molecular weight obtained from SAXS and g.p.c. data is certainly due to the polydispersity of the PEO samples. Indeed, the g.p.c. trace of PEO6K shows a relatively low molecular tail which lowers the number-average molecular weight value. Two important conclusions can be drawn from the agreement between these $< M_n >$ values obtained from SAXS and g.p.c. data: (i) the chain axes of the PEO macromolecules are normal to the basal planes of the lamellar crystals of PEO6K–PDCL molecular complex; (ii) the thickness of the amorphous layer (L_a) is very small compared to the thickness of the crystalline core (L_c). A careful examination of the SAXS intensity curves of *Figure 11*a shows that the first-order diffraction peak has a lower intensity than the second-order for crystallization at 30°C. The same comment can be made for the third and the fourth orders at the same crystallization temperature. The ratio of the intensity of the first and second orders increases with the crystallization temperature. The occurrence of extended chain (EC) and one-integral-folded chain (1-IFC) crystals

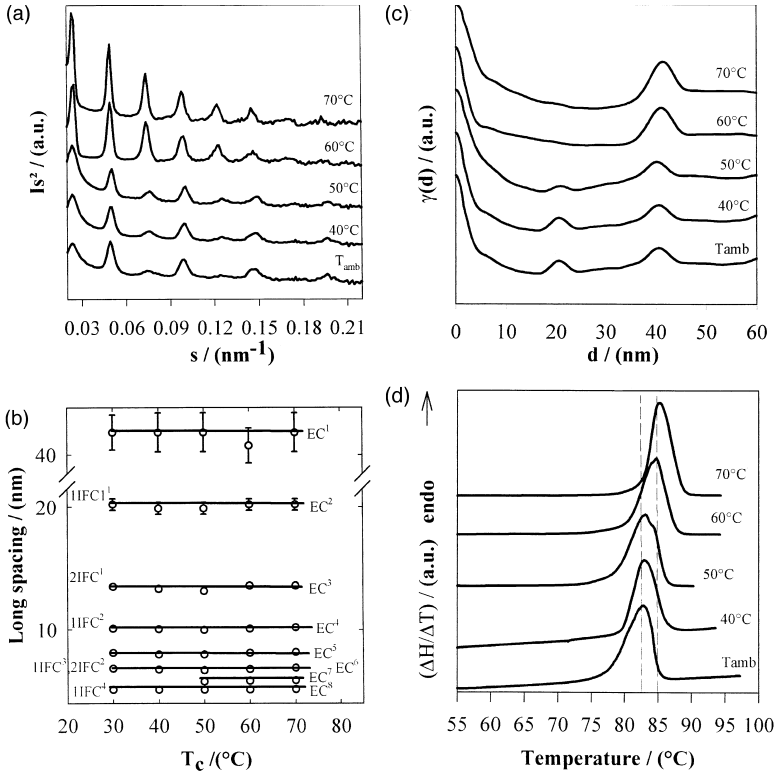

Figure 11 (a) Lorentz corrected SAXS intensity curves of the PEO6K–PDCL molecular complex crystallized at various crystallization temperatures between 25 and 70°C. The values of the crystallization temperatures are indicated on the right side of the figure. (b) Long spacings of lamellar crystals of PEO6K–PDCL molecular complex *versus* the crystallization temperature. EC and *x*-IFC are used for 'extended chains' and *x*-times integral-folded chains; the subscript represents the order of the diffraction (EC^3 means the third order of the long spacing corresponding to EC crystals; 2-IFC^2 means the second order of the long spacing of two-folded chain crystals). (c) Correlation functions of SAXS intensity curves of PEO6K–PDCL samples crystallized at various temperatures given in the figure. (d) Melting curves of PEO6K–PDCL samples crystallized at various temperatures. The values of the crystallization temperatures are given in the figure

in the PEO6K–PDCL molecular complex crystallized at low temperatures can be accounted for by the two experimental observations reported above. Indeed, as the thickness of the amorphous regions is very small, the second SAXS peak (20.5 nm) can correspond to the second order of the lamellar thickness of EC crystals and also to the first order of the thickness of 1-IFC crystals. The correlation functions have been calculated from the SAXS intensity curves. The correlation functions of samples crystallized at room temperature, 40 and 50°C clearly show a peak centred around 20 nm which supports the conclusion given above. Unlike PEO6K oligomers, where EC crystals are only observed for crystallization temperatures near the melting temperature ($T_c > 53$°C), extended chain crystals of the PEO6K–RES molecular complex can be obtained in a wide range of crystallization temperatures (30 to 70°C). The melting curve of the PEO6K–PDCL molecular complexes crystallized below 40°C, and at 70°C contained only one endotherm. The temperature of the extremum is 82.9 and 85°C for crystallization temperatures of 40 and 70°C, respectively (*Figure 11*d). A shoulder is present on the right side of the melting endotherm of PEO6K–PDCL samples crystallized at 50 and 60°C. This shoulder increases in magnitude with crystallization temperature. From the SAXS results given above, the endotherms at 82.9 and 85°C result from the melting of 1-IFC and EC lamellar crystals, respectively.

PEO6K–RES molecular complex. Some Lorentz corrected SAXS intensity curves obtained from PEO6K–RES molecular complexes crystallized from the melt between 30 and 70°C are shown in *Figure 12*a. These SAXS intensity curves contain five well-resolved diffraction peaks. Their long spacings are equal to 38, 18.7, 12.3, 9.1 and 7.3 nm, respectively, and appear to be independent of the crystallization temperature (*Figure 12*b). These peaks are the five first orders of the long spacing corresponding to a full extended chain conformation for PEO6K in the molecular complex. Indeed, the molecular weight ($< M_n^* >$) estimated from the long spacing $L = 38$ nm is equal to 6950, i.e. a slightly higher value than the value obtained by g.p.c. A careful examination of the magnitude of the SAXS intensity maxima (*Figure 12*a) indicates that the ratio of the intensity of the first and second orders increases with the crystallization temperature, showing that PEO6K–RES samples crystallized near room temperature contain a mixture of 1-IFC and EC lamellar crystals. The correlation functions calculated from the intensity SAXS curves exhibit two well-differentiated maxima at 19 and 38 nm for molecular complex crystallized at 30, 40 and 50°C which correspond to the thickness of 1-IFC and EC lamellar crystals, respectively (*Figure 12*c). The fraction of EC crystals increases with the crystallization temperature. Further support for the presence of a mixture of EC and IFC crystals in PEO6K–RES samples crystallized in this temperature range has been obtained from the analysis of their melting curves (*Figure 12*d). These curves contain several melting peaks (or shoulders) and can be used, in principle, to estimate the proportion of EC and *x*-IFC crystals. The different melting temperatures T_m depend very slightly on the crystallization temperature T_c as expected for such EC and IFC lamellar crystals. The occurrence of several melting peaks in the d.s.c. trace confirms the result of the simultaneous presence

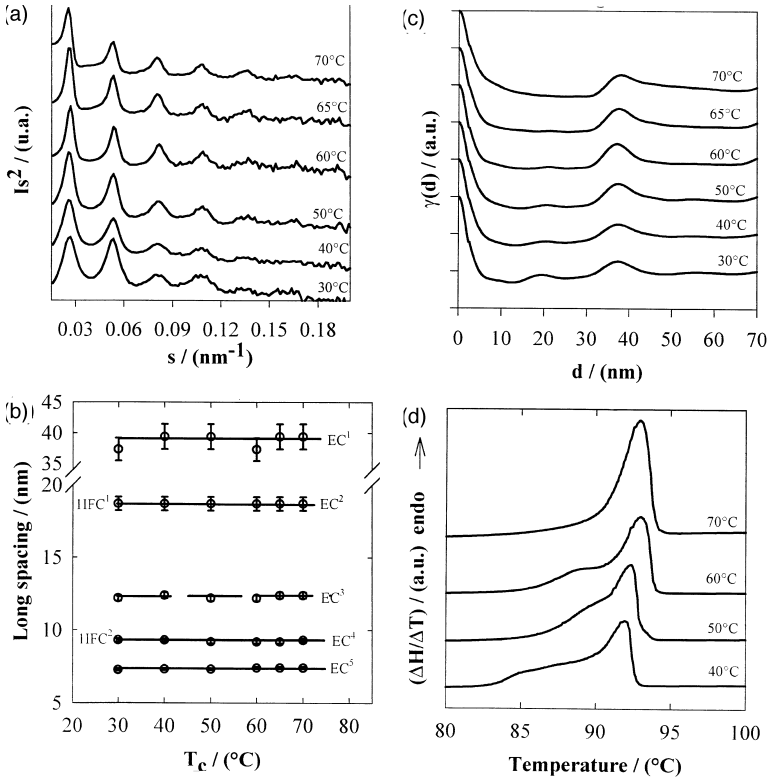

Figure 12 (a) Lorentz corrected SAXS intensity curves of the PEO6K–RES molecular complex crystallized at various crystallization temperatures between 30 and 70°C. The values of the crystallization temperatures are indicated on the right side of the figure. (b) Long spacings of lamellar crystals of the PEO6K–RES molecular complex *versus* the crystallization temperature. EC and 1-IFC are used for 'extended chains' and one-integral folded chains; the subscript represents the order of the diffraction (EC^3 means the third order of the long spacing corresponding to EC crystals; $1\text{-}IFC^2$ means the second order of the long spacing of one-folded chain crystals). (c) Correlation functions of SAXS intensity curves of the PEO6K–RES samples crystallized at various temperatures given in the figure. (d) Melting curves of PEO6K–RES samples crystallized at various temperatures. The values of the crystallization temperatures are given in the figure

of lamellar crystals with quite different thicknesses for almost all crystallization temperatures obtained from the SAXS intensity data: (i) at low crystallization temperatures, the PEO–RES spherulites are made up of at least three types of lamellar crystals, EC, 1-IFC and 2-IFC; (ii) at high crystallization temperatures, i.e. for $T_c \geq 70$°C, only EC crystals are present; (iii) spherulitic samples crystallized between 40 and 70°C are mixtures of EC and IFC lamellar crystals—the proportion of EC crystals increases continuously with the crystallization temperature. The equilibrium melting temperatures of these crystals are estimated to be 94.2, 91.6 and 89.3°C for EC, 1-IFC and 2-IFC crystals, respectively. Despite the increase of the melting temperature of the PEO molecular complexes with respect to the melting temperature of pure PEO oligomers, the difference between the melting temperatures of EC to 1-IFC crystals is around 3°C, a value similar to that reported for pure PEO6K oligomers (the melting temperatures of EC and 1-IFC PEO crystals are 63.3 and 60.7°C, respectively[10–12]).

PEO6K–HYD molecular complex. Some typical Lorentz corrected SAXS intensity curves obtained from PEO6K–HYD molecular complexes crystallized from the melt between room temperature and 70°C are shown in *Figure 13*a. These SAXS intensity curves contain three resolved diffraction peaks. Their long spacings are equal to 36.7, 18.7 and 12.4 nm, respectively, and also appear to be independent of the crystallization temperature (*Figure 13*b). These peaks are the first three orders of the long spacing corresponding to a full extended chain conformation of PEO in the molecular complex. The integrated intensity of the second peak at 18.7 nm is much larger than that of the first peak at 36.7 nm, which indicates that PEO6K–HYD samples crystallized at room temperature contain mixtures mainly of 1-IFC crystals and of a small amount of EC lamellar crystals. The analysis of the correlation functions calculated from the intensity SAXS (*Figure 13*c) leads to the same conclusion. The fraction of EC crystals increases with the crystallization temperature. The melting curves of PEO–HYD samples crystallized between room temperature and 70°C are given in *Figure 13*d. The melting temperature (temperature of the extremum of the endotherm) shifts from 82.7 to 85.1°C for PEO–HYD samples crystallized at room temperature and at 70°C, respectively. A more careful d.s.c. analysis, using different heating rates, seems to be necessary to identify the melting of 1-IFC and EC lamellar crystals.

PEO6K–PNP molecular complex. Lorentz corrected SAXS intensity curves of PEO6K–PNP crystallized from the melt between 30 and 70°C are shown in *Figure 14*a. All the SAXS intensity curves exhibit only two broad peaks characteristic of a wide distribution of lamellar thicknesses. The correlation functions calculated from each SAXS curve are given in *Figure 14*b. The long spacings obtained from the Lorentz corrected SAXS curves and the correlation functions are given in *Figure 14*c. There is good agreement between the values of the long spacing obtained from the correlation function and from the Lorentz corrected SAXS intensity curves: the largest deviation is 0.5 nm. The two

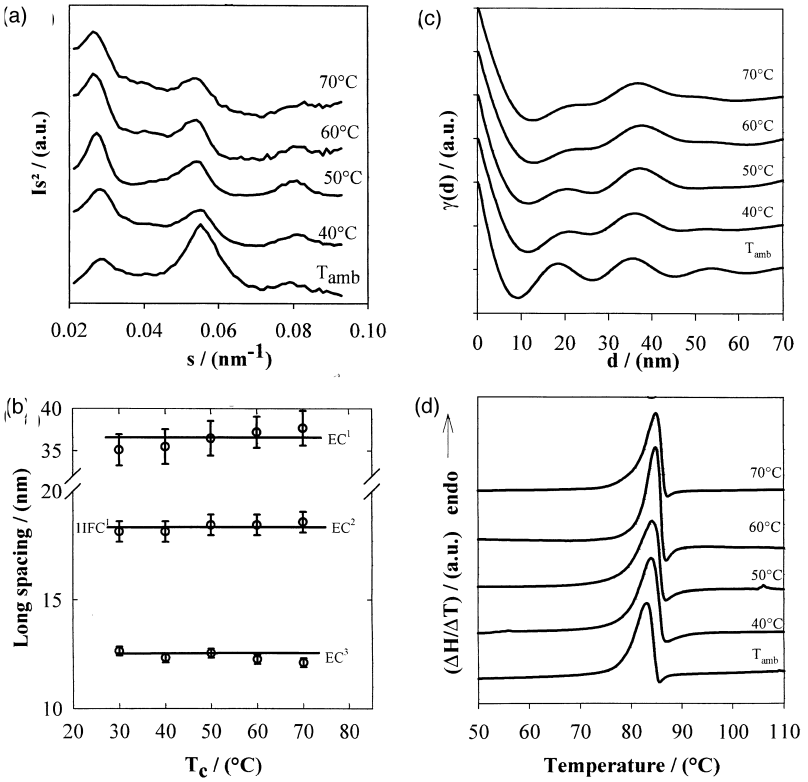

Figure 13 (a) Lorentz corrected SAXS intensity curves of PEO6K–HYD molecular complex crystallized at various crystallization temperatures between room temperature and 70°C. The values of the crystallization temperatures are indicated on the right side of the figure. (b) Long spacings of lamellar crystals of the PEO6K–HYD molecular complex *versus* the crystallization temperature. EC and 1-IFC are used for 'extended chains' and one-integral-folded chains; the subscript represents the order of the diffraction as described previously. (c) Correlation functions of SAXS intensity curves of PEO6K–HYD samples crystallized at various temperatures given in the figure. (d) Melting curves of PEO6K–HYD samples crystallized at various temperatures given in the figure

long spacings obtained from the Lorentz corrected SAXS curves correspond to the two first orders of the same lamellar thickness. The long spacing of the PEO6K–PNP lamellar crystals increases with the crystallization temperature from 8.2 to 12.3 nm (*Figure 14*c). Surprisingly, neither EC nor IFC crystals are observed for the PEO–PNP complexes prepared from PEO6K. Taking into account the length of extended chains of PEO6K, these long spacings data imply that the PEO–PNP spherulitic samples are made up of NIFC crystals.

The melting curves of PEO6K–PNP samples crystallized at various temperatures ranging from 40 to 70°C are given in *Figure 14*d. Only a single endotherm is observed over all the crystallization temperature range studied. Moreover, the melting temperature T_m monotonically increases against the crystallization temperature, as expected for NIFC crystals. The estimated equilibrium melting temperature (T_m^0) of PEO6K–PNP crystals from the Hoffman–Weeks procedure[47] is 104°C.

The morphological observations made from the analysis of SAXS, WAXD and d.s.c. data on PEO molecular complexes crystallized for very long times are summarized in *Table 3* together with the conclusions obtained from the analysis of time-resolved SAXS measurements of the early stage of crystallization from the melt. As a rule, the samples of PEO6K–PDCL, PEO6K–RES and PE06K–HYD molecular complexes crystallized at room temperature to 50–60°C for long times consist of mixtures of IFC and EC crystals. For the PEO–HYD molecular complex, IFC crystals are always present with EC crystals even at the highest investigated crystallization temperature. No NIFC crystals remain in samples of PEO–molecular complexes crystallized at room temperature except for the PEO–PNP molecular where NIFC crystals occur at all the range of crystallization temperatures. Even if the crystal structure is different, all these molecular complexes are characterized by an alternate structure of layers of PEO and benzenic molecules. As spherulitic samples have been investigated, the growth faces of crystals of these molecular complexes cannot be determined precisely. It seems more relevant to relate the differences observed in the morphology of these lamellar crystals of PEO molecular complexes to the type and magnitude of the interactions between host and guest molecules. The interaction between *p*-dihalogenobenzene molecules and PEO chains is weakest. These molecular complexes, particularly the PEO–PDCL complex, have been described as 'intercalates'[24]. Hydrogen bonds between guest and host molecules are a general characteristics of the three other molecular complexes presently investigated (PEO–RES, PEO–HYD and PEO–PNP). Two experimental parameters allow one to obtain qualitative information about the magnitude of the interactions between host and guest molecules for these three molecular complexes: the melting temperature of the molecular complexes (*Table 1*) and the value of the wavenumber of the ν_{OH} stretching (*Table 3*). PEO–RES and PEO–PNP molecular complexes crystallize as NIFC crystals in the early stage of crystallization from the melt. As the degree of crystallinity estimated from time-resolved WAXD intensity measurements has reached its maximum after 2 to 3 min of crystallization, the magnitude of the interactions in the molecular complexes seems to be a determining factor for the transformation rate of NIFC into IFC crystals. The rate of transformation of NIFC into IFC crystals is very slow for

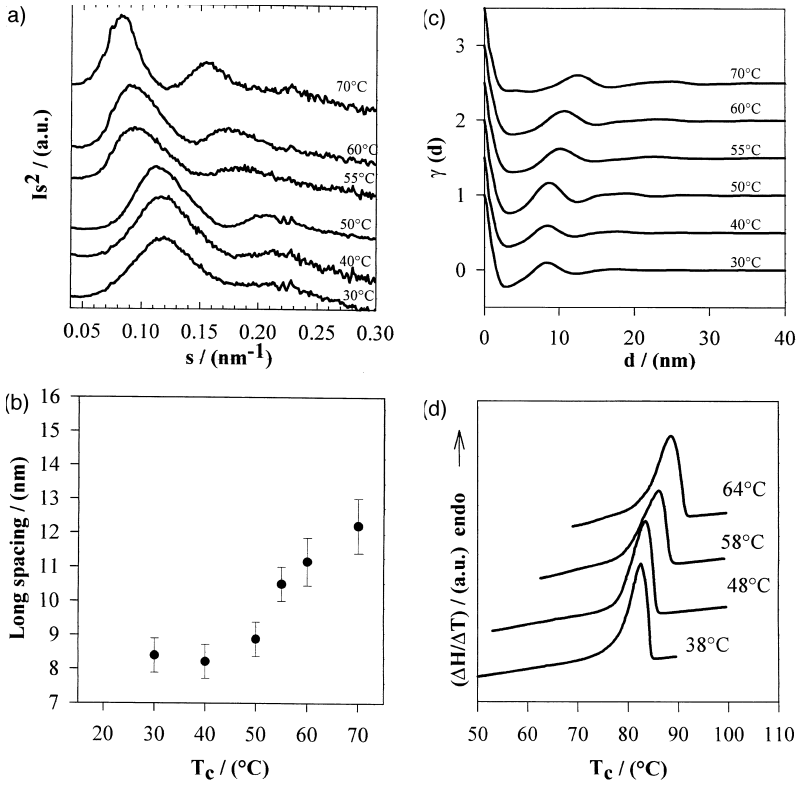

Figure 14 (a) Lorentz corrected SAXS intensity curves of the PEO6K–PNP molecular complex crystallized at various crystallization temperatures between 30 and 70°C. The values of the crystallization temperatures are indicated on the right side of the figure. (b) Correlation functions of SAXS intensity curves of PEO6K–PNP samples crystallized at various temperatures given in the figure. (c) First and second orders of the long spacing of lamellar crystals of PEO6K–PNP molecular complex *versus* the crystallization temperature. Filled symbols represent data obtained from the Lorentz corrected SAXS curves. Open circles represent data obtained from the correlation function. (d) Melting curves of PEO6K–HYD samples crystallized at various temperatures. The values of the crystallization temperatures are given on the left side of the figure

systems where the interactions between host and guest molecules are strong. These interactions are strongest in the PEO–PNP molecular complex and weakest in the PEO–HYD molecular complex.

Metastability of the PEO–RES molecular complex

Large spherulites of PEO6K molecular complexes of diameter about 10 mm can be obtained by crystallization from the melt, which indicates that the primary nucleation density of these systems is very low. An optical micrograph showing unbanded and banded spherulites of the PEO–RES molecular complex is given in *Figure 15*. Between crossed polaroids, the unbanded and banded spherulites reveal a dark Maltese cross pattern along the vibration directions of the polarizer and the analyser. The PEO–RES unbanded spherulites are negatively birefringent and their melting temperature, determined by optical microscopy, ranges between 93 and 95°C. Banded spherulites reveal alternating circular narrow positive and wide negative birefringent bands, separated by extinction lines. The melting temperature of the PEO–RES banded spherulites is 71°C[34]. The banded spherulites are metastable at room temperature and transform into unbanded spherulites[35]. Two different phenomena are observed during the simultaneous growth of unbanded and banded spherulites at a given crystallization temperature: an overgrowth rate of the fastest, namely the unbanded, form along the interface of the banded-form, and a transformation of the banded-form into the unbanded-form, which propagates as a dynamic front at constant rate G_t. As the growth rates of both forms differ, the boundary between these two types of spherulites consists of an arc of Descartes's oval connected to two arcs of a logarithmic spiral as described elsewhere[34]. In banded spherulites, it is generally admitted that the extinction pattern results from a periodic variation of the refractive indexes of the crystals along the radius of the spherulite and the optical pitch of the twist depends on the crystallization temperature[48]. *Figure 16* is an optical micrograph of a part of a ringed spherulite crystallized at different temperatures (20, 40, 20, 60 and 20°C) showing that the optical period increases with crystallization temperature. The optical ring spacing data for banded spherulites are plotted against the crystallization temperature in *Figure 17*. As no SAXS and WAXD patterns of part of a banded spherulite are presently available, we are only in a position to establish a comparison between the crystallization behaviour of the PEO–RES molecular complex and ultralong paraffins. Indeed, it has recently been shown that folded chain and extended chain lamellar crystals of ultralong paraffins crystallize as banded and unbanded spherulites, respectively[49].

CONCLUSION

In the early stage of crystallization, PEO–RES, PEO–HYD and PEO–PNP molecular complexes form NIFC crystals, except for the PEO–HYD molecular complex which forms *x*-IFC crystals. However, unlike the NIFC crystals observed in pure PEO oligomers, the NIFC crystals of PEO6K–RES, PEO–HYD are relatively 'stable' and slowly transform into IFC or EC crystals. Therefore, NIFC, IFC and EC lamellar crystals can be present in the same sample of the PEO–RES

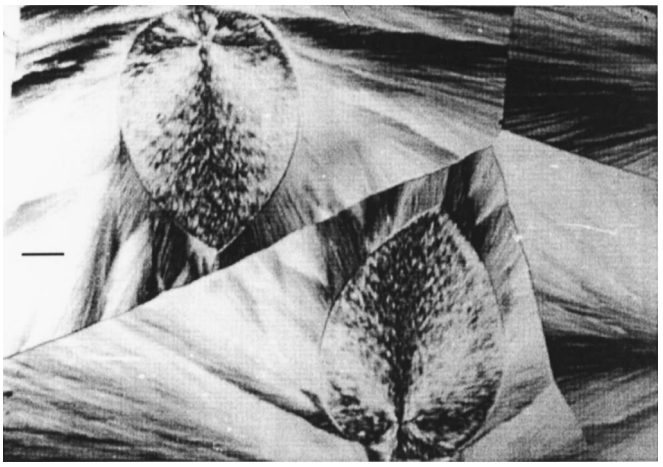

Figure 15 Optical micrograph showing unbanded and banded spherulites of the PEO6K–RES molecular complex. The scale bar represents 100 μm

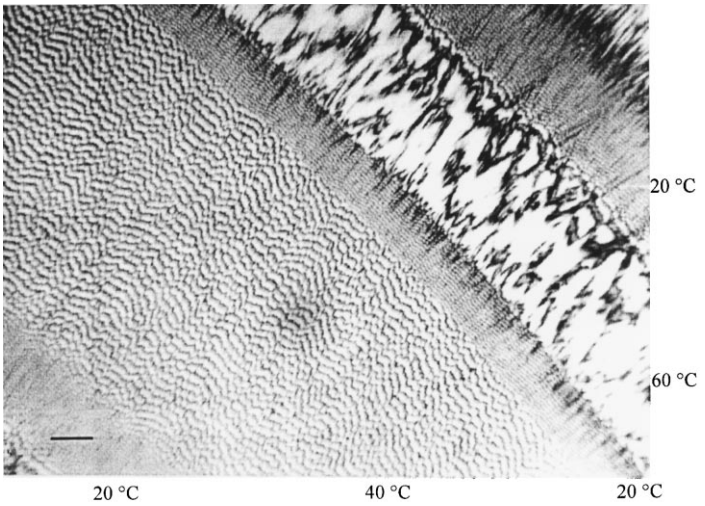

Figure 16 Optical micrograph of banded spherulites crystallized step by step at

molecular complex, depending upon the crystallization temperature and the crystallization time. NIFC crystals of molecular complexes can be observed in a broader range of crystallization temperatures than for pure PEO. The NIFC crystals of the PEO–PNP molecular complex do not transform into IFC crystals even after long crystallization times. The magnitude of the interactions between host and guest molecules in these molecular complexes, estimated from the OH stretching infrared bands, allows one to account for the relative stability of the NIFC crystals. It has also been demonstrated experimentally that ringed spherulites of PEO–RES molecular complexes are metastable and transform into unbanded spherulites. The analogy with the morphology of spherulites of ultralong paraffins, where it has been reported that chain-folded crystals and chain-extended crystals are present in ringed and unbanded spherulites, respectively, needs to be clarified by micro-WAXD and micro-SAXS measurements on part of a ringed spherulite.

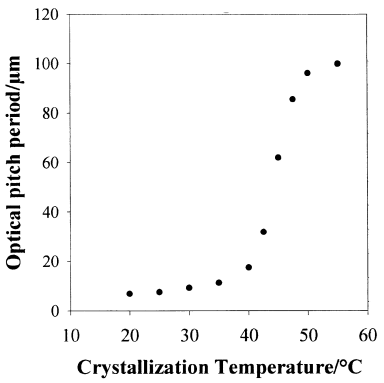

Figure 17 Optical period of banded spherulites of PEO6K–RES *versus* the crystallization temperature

ACKNOWLEDGEMENTS

This work was supported by the Belgian National Funds for Scientific Research and the Science Program of the European Union for Access to the Synchrotron Radiation Facilities at LURE (Centre Universitaire de Paris-Sud, Orsay, France). Dr C. Bourgaux is thanked for technical assistance during the SAXS experiments on the D23 beam line at LURE.

REFERENCES

1. Keller, A., *Philos. Mag.*, 1957, **2**, 1171.
2. Tadokoro, H., Chatani, Y., Yoshihara, T., Tahara, S. and Murahashi, S., *Makromol. Chem.*, 1964, **73**, 109.

3. Takahashi, Y. and Tadokoro, H., *Macromolecules*, 1973, **6**, 359.
4. Arlie, J.P., Spegt, P. and Skoulios, A., *Makromol. Chem.*, 1966, **99**, 160.
5. Arlie, J.P., Spegt, P. and Skoulios, A., *Makromol. Chem.*, 1967, **104**, 104.
6. Spegt, P., *Makromol. Chem.*, 1970, **140**, 167.
7. Hartley, A., Leung, Y.K., Booth, C. and Sheppard, I.W., *Polymer*, 1988, **29**, 579.
8. Kovacs, A.J. and Gonthier, A., *Kolloid Z. Z. Polym.*, 1972, **250**, 530.
9. Song, K. and Krimm, S., *Macromolecules*, 1990, **23**, 1946.
10. Buckley, C.P. and Kovacs, A.J., *Prog. Colloid Polymer Sci.*, 1975, **58**, 44.
11. Buckley, C.P. and Kovacs, A.J., *Colloid Polymer Sci.*, 1976, **254**, 695.
12. Buckley, C. P. and Kovacs, A. J., in *Structure of Crystalline Polymers*, ed. I. H. Hall, 1984, pp. 261–307.
13. Song, K. and Krimm, S., *Macromolecules*, 1989, **22**, 1504.
14. Cheng, S.Z.D., Zhang, A. and Chen, J.J., *J. Polym. Sci., Polym. Lett.*, 1990, **28**, 233.
15. Cheng, S. Z. D., Chen, J. J., Wu, S. X., Zhang, A., Yandrasatis, M. A., Zhuo, R., Quirk, R. P., Habenschuss, A. and Zschack, P. R., *Crystallization of Polymers*, NATO Series C405, ed. M. Dosière, 1993, p. 51.
16. Cheng, S.Z.D., Chen, J., Zhang, A. and Herberer, D.P., *J. Polym. Sci., Polym. Phys.*, 1991, **29**, 299.
17. Cheng, S.Z.D., Wu, S.S., Chen, J., Zhuo, Q., Quirk, R.P., von Meerwall, E.D., Hsiao, B.S., Habenschuss, A. and Zschack, P.R., *Macromolecules*, 1993, **26**, 5105.
18. Kim, I. and Krimm, S., *Macromolecules*, 1994, **27**, 5232.
19. Guenet, J.-M., *Thermoreversible Gelation of Polymers and Biopolymers*, Academic Press, London, 1992.
20. Parrod, J., Kohler, A. and Hild, G., *Compt. Rend.*, 1958, **246**, 1046.
21. Tadokoro, H., Yoshihara, T., Chatani, Y. and Murahashi, S., *J. Polym. Sci. B*, 1964, **2**, 363.
22. Bailey, F.E. and France, H.G., *J. Polym. Sci.*, 1961, **49**, 397.
23. Parrod, J., Kohler, A. and Hild, G., *Makromol. Chem.*, 1964, **75**, 52.
24. Point, J.-J. and Coutelier, C., *J. Polym. Sci., Polym. Phys. Ed.*, 1985, **23**, 231.
25. Point, J.-J., Jasse, B. and Dosière, M., *J. Phys. Chem.*, 1986, **90**, 3273.
26. Point, J.-J., Coutelier, C. and Villers, D., *J. Phys. Chem.*, 1986, **90**, 3277.
27. Point, J.-J. and Demaret, Ph.D., *J. Phys. Chem.*, 1987, **91**, 797.
28. Point, J.-J. and Damman, P., *Macromolecules*, 1991, **24**, 2019.
29. Point, J.-J., Damman, P. and Guenet, J.-M., *Polymer Communications*, 1991, **32**, 477.
30. Myasnikova, R.M., *Vysokomol. Soyed.*, 1977, **A19**, 564.
31. Myasnikova, R.M., Titova, E.F. and Obolonkova, E.S., *Polymer*, 1980, **21**, 403.
32. Skazka, V.S., Nikolayev, Y., Bekturov, Y.A., Kudaibergenov, S., Petrenko, K.D. and Privalko, V.P., *Polymer Sci. USSR*, 1986, **28**, 2128.
33. Belfiore, L.A., Lutz, T.J., Cheng, C. and Bronnimann, C.E., *J. Polym. Sci., Polym. Phys.*, 1990, **28**, 1261.
34. Delaite, E., Point, J.-J., Damman, P. and Dosière, M., *Macromolecules*, 1992, **25**, 4768.
35. Villers, D., Dosière, M. and Paternostre, L., *Polymer*, 1994, **35**, 1586.
36. Cheng, C. and Belfiore, L.A., *Polymer Preprints*, 1989, **30**(2), 325.
37. Belfiore, L.A. and Ueda, E., *Polymer*, 1992, **33**, 3833.
38. Paternostre, L., Damman, P. and Dosière, M., *Macromol. Symp.*, 1997, **114**, 205.
39. Paternostre L., Damman, P., Dosière, M., *J. Polym. Sci., Polym. Phys. Ed.*, submitted.
40. Point, J.-J. and Damman, P., *Macromolecules*, 1992, **25**, 1184.
41. Damman, P. and Point, J.-J., *Macromolecules*, 1993, **26**, 1722.
42. Damman, P. and Point, J.-J., *Macromolecules*, 1994, **27**, 3919.
43. Dosière, M., *J. Macromol. Sci.*, 1996, **B35**, 303.
44. Dosière, M., *Macromol. Symp.*, 1997, **114**, 51.
45. Paternostre, L., Damman, P., Dosière, M. and Bourgaux, C., *Macromolecules*, 1996, **29**, 2046.
46. Paternostre, L., Damman, P. and Dosière, M., *Macromolecules*, 1997, **30**, 3946.
47. Hoffman, J.D. and Weeks, J.J., *J. Chem. Phys.*, 1965, **142**, 4301.
48. Lindenmeyer, P.H. and Holland, V.F., *J. Appl. Phys.*, 1964, **35**, 55.
49. Bassett, D.C., Olley, R.H., Sutton, S.J. and Vaughan, A.S., *Macromolecules*, 1996, **29**, 1852–1853.